Journal of Computational Physics, 230 (4), 2011, pp. 1439–1453.

Generalized Ohm's Law and Potential Equation in Computational Weakly-Ionized Plasmadynamics

Bernard Parent[*], Mikhail N. Shneider[†], and Sergey O. Macheret[‡]

A variant of the generalized Ohm's law that is suited for a weakly-ionized multicomponent plasma in a magnetic field is here derived. The latter takes into consideration the current due to the non-neutrality of the plasma, the current due to the Hall effect, and the currents due to the ion slip associated with each type of ion. An equation for the electric field potential applicable to a non-neutral multicomponent plasma in the presence of a magnetic field is then presented. Despite some similarities between the potential equation and the Poisson equation, it is argued that the discretization of the potential equation cannot be accomplished in the same manner by using only central differences. It is here proven (and subsequently verified through a test case) that when the plasma exhibits conjunctly a high Hall parameter and a high electrical conductivity gradient, the centered stencils introduce spurious oscillations which can lead to severe numerical error. A novel discretization of the potential equation consisting of a blend of central and upwind differences is then presented. The proposed scheme is consistently monotonic for any value of the Hall parameter and is second-order accurate except in the vicinity of discontinuities.

1. Introduction

SEVERAL applications of weakly-ionized plasma technologies for improving the performance of aircraft have recently been the subject of considerable interest. One possible application is aerodynamic flow control through virtual bodies created by heat deposition using electron beams or another type of external ionizer [1, 2]. Other applications are centered on the force exerted on the airflow due to magnetohydrodynamic interaction (MHD) or electrohydrodynamic interaction (EHD). The EHD interaction (or *ion wind*) is suspected to be one of the mechanisms responsible for the high success of plasma actuators in preventing or delaying boundary layer separation [3], in enhancing jet mixing [4], in keeping the flow attached on turbine blades [5], or in controlling the vortices above a delta wing [6]. On the other hand, the MHD interaction could be useful in controlling the inlet flowfield [7, 8], in suppressing boundary-layer separation [9], in imparting momentum to a gas [10, 11], or in generating electrical power aboard a flight vehicle through a MHD generator [12, 13].

Despite some success using the weakly-ionized plasma technologies, there remain several key physical phenomena that are still not well understood. For instance, it is not clear whether plasma actuators achieve flow control through the EHD interaction or through heating, or how much of the Joule heating losses observed in a MHD generator occur within the plasma sheath. To obtain a better understanding of the physical phenomena, it is desirable to obtain more detailed computational results.

A computational study of plasmas generally requires the coupled solution of the Navier-Stokes equations to obtain the bulk flow properties and of the Maxwell equations to obtain the electric and magnetic field distributions. However, when a plasma is weakly-ionized (that is, when the fraction of the gas molecules that are ionized are in the range 10^{-8} to 10^{-4}) and when the applied magnetic field does not vary in time, it can be shown that the sole solution of the electric field potential provides a reasonable approximation to the electromagnetic fields. The potential equation is derived from the so-called "generalized

[*]Faculty Member, Dept. of Aerospace Engineering, Pusan National University, Busan 609-735, Korea, http://www.bernardparent.com.

[†]Senior Research Scientist, Dept. of Mechanical and Aerospace Engineering, Princeton University, Princeton, NJ 08544-5263, USA.

[‡]Senior Research Scientist, Dept. of Mechanical and Aerospace Engineering, Princeton University, Princeton, NJ 08544-5263, USA. Current address: Lockheed Martin Aeronautics Company, 1011 Lockheed Way, Palmdale, California 93599-0160.

Ohm's law" which provides an algebraic expression linking the current density to the electric and magnetic fields [14]:

$$\boldsymbol{J} = \sigma(\boldsymbol{E} + \boldsymbol{V} \times \boldsymbol{B}) - \underbrace{\frac{\beta_\mathrm{e}}{|\boldsymbol{B}|}\boldsymbol{J} \times \boldsymbol{B}}_{\text{Hall current}} + \underbrace{\frac{\beta_\mathrm{e}\beta_\mathrm{i}}{|\boldsymbol{B}|^2}(\boldsymbol{J} \times \boldsymbol{B}) \times \boldsymbol{B}}_{\text{current due to ion slip}} \tag{1}$$

with σ the conductivity and with β_i and β_e the Hall parameter for the ions and the electrons, respectively. The latter form of the generalized Ohm's law (or a variant including the effect of the electron pressure gradient) is the backbone of the recent numerical methods solving weakly-ionized flowfields. However, while Eq. (1) takes into account the Hall effect as well as the ion slip effect, it suffers from the limitation of being applicable to a plasma in which only one type of positive ion exists alongside the electrons. This can be problematic when used in conjunction with fluid flow solvers that include 3 or more charged species. Several attempts have been made to overcome this shortcoming (see for instance Ref. [15, p. 361] and more recently Refs. [16, 17]). However, the latter fell short of yielding a closed-form expression for the current that is specifically tailored to a weakly-ionized gas and that can be readily implemented in a CFD code.

The first part of this paper hence consists of presenting a derivation of a variant of the generalized Ohm's law that is specifically suited to a weakly-ionized multicomponent plasma. The form of the generalized Ohm's law presented herein takes into consideration the Hall current as well as the separate ion slip currents associated with each type of ion. The second part of this paper presents a novel discretization of the electric field potential. The discretization of the potential equation has so far been accomplished through second-order accurate centered stencils (see Refs. [13, 18] for instance). This has proven to be a successful strategy. Indeed, the potential equation can be written as a diffusion equation, and the diffusion derivatives can generally be discretized successfully using centered stencils. But, as will be proven subsequently in this paper, this discretization approach fails when the plasma exhibits conjunctly a high Hall parameter and a high electrical conductivity gradient. In the plasma regions with such characteristics, the centered stencils introduce spurious oscillations which can lead to severe numerical error. As a remedy for this problem, a new discretization stencil for the potential equation is here proposed. The proposed scheme is consistently monotonic for any value of the Hall parameter and is second-order accurate except in the vicinity of discontinuities.

2. Plasma Conservation Equations

Despite its name, the generalized Ohm's "law" is not strictly a law because it can be derived from more basic physical principles. These more basic physical principles are the principle of conservation of mass and the principle of conservation of momentum applied to each charged species. In this section, a short outline of the momentum and mass conservation equations of the plasma species is given, along with simplified forms applicable to a weakly-ionized plasma.

2.1. Charged Species Momentum Conservation

Denoting a particular species with the subscript/superscript k, the inviscid form of the momentum equation can be written as:

$$m_k N_k \frac{\partial \boldsymbol{V}^k}{\partial t} + m_k N_k \boldsymbol{V}^k \cdot \nabla \boldsymbol{V}^k = C_k N_k (\boldsymbol{E} + \boldsymbol{V}^k \times \boldsymbol{B}) - \frac{|C_k| N_k}{\mu_k} \left(\boldsymbol{V}^k - \boldsymbol{V}^\mathrm{n}\right) - \nabla P_k \tag{2}$$

with m_k the mass of the ion or electron, C_k is the charge of the ion or electron under consideration (equal to $-e$ for the electrons, $+e$ for the singly-charged positive ions, $-e$ for the singly-charged negative ions, $-2e$ for the doubly-charged negative ions, etc.), $\boldsymbol{V}^k$ the species velocity (including drift and diffusion), $\boldsymbol{V}^\mathrm{n}$ the velocity of the neutrals, μ_k the species mobility, N_k the species number density, ∇P_k the pressure gradient vector of the species under consideration, $\boldsymbol{E}$ the electric field vector, and $\boldsymbol{B}$ the magnetic field vector.

In the latter, the forces originating from the shear stresses and from the collisions between charged species are assumed to be negligible compared to the forces originating from the collisions of the charged species with the neutrals. The latter are good assumptions for a weakly-ionized gas. Indeed, should the ionization fraction be less than 10^{-4}, it can be shown that the force due to collisions between charged species would amount to less than 1% of the force induced by ion-neutral or electron-neutral collisions, and that the force resulting from the shear stresses would typically amount to an even smaller quantity.

It is noted that the terms including the pressure gradients are retained. Indeed, it can be shown that the change in momentum due to the ion and electron pressure gradients is not always negligible for weakly-ionized gases. For instance, not only do the

charged species pressure gradients become substantial within the cathode sheaths, but the pressure gradients can also be of importance in the vicinity of shockwaves and in regions with low gas density.

Nonetheless, it can be shown that the forces due to pressure gradients are unlikely to exceed significantly the electromagnetic forces for typical flowfields. Then, taking this into consideration, a simple derivation shows that the change in inertia of the electrons can be assumed negligible as long as the following restrictions are met:

$$T_\mathrm{e} < 60,000\,\mathrm{K} \tag{3}$$

and

$$\left|\frac{1}{P_\mathrm{e}}\nabla P_\mathrm{e}\right| \ll \frac{|C_\mathrm{e}|}{\mu_\mathrm{e}\sqrt{m_\mathrm{e}k_\mathrm{B}T_\mathrm{e}}} \tag{4}$$

with T_e the electron temperature, m_e the mass of the electron, and k_B the Boltzmann constant. The restriction on the electron temperature is easily satisfied in most weakly-ionized airflow problems. Indeed, even under very high electromagnetic fields, the electron temperature rarely exceeds 30,000 K. As for the restriction on the gradient of the electron pressure gradient, it would become invalid only if the electron pressure varies abruptly over a distance of less than one micrometer (in sea-level air). This is unlikely to occur due to the strong electron diffusion effectively prohibiting any such sudden change in the electron properties.

Further, it can be proven that the change in inertia of the ions can be assumed negligible compared to the ion pressure gradient as long as

$$\frac{|\boldsymbol{E}^\mathrm{i}|}{N} \ll \left(\frac{k_\mathrm{B}T^2}{T_\mathrm{ref}N_\mathrm{ref}^2 m_\mathrm{i}(\mu_\mathrm{i})_\mathrm{ref}^2}\right)^{\frac{1}{2}} \tag{5}$$

Alternately, the change in ion inertia can be assumed negligible compared to the electric field force if the following is true

$$\frac{|N_\mathrm{i} - N_\mathrm{e}|}{N} \ll \frac{\epsilon_0}{m_\mathrm{i}(\mu_\mathrm{i})_\mathrm{ref}^2 N_\mathrm{ref}}\frac{P}{P_\mathrm{ref}} \tag{6}$$

with $\boldsymbol{E}^\mathrm{i}$ the electric field in the ion frame of reference, N the number density of the bulk of the plasma, m_i the mass of the ion, ϵ_0 the permittivity of free space, P the pressure of the bulk of the gas, and $(\mu_\mathrm{i})_\mathrm{ref}$ the ion mobility evaluated at a reference temperature T_ref, at a reference pressure P_ref and at a reference number density N_ref. Because both the pressure gradient and electric field terms are kept in the momentum equation, only one of the above two conditions needs to be met for the ion inertia to be considered negligible. Then, from Eqs. (5) and (6), it can be easily deduced that for air plasmas at a pressure varying between 0.01 and 1 atm, the change in inertia of the ion N_2^+ would become of importance only when three conditions are found conjunctly: (i) the reduced electric field is in the order of 10^{-19} V m^2 or more, and (ii) the plasma has significant non-neutrality, and (iii) the ionization fraction is more than 10^{-6}–10^{-4}. Except perhaps in the cathode sheath, such is unlikely to occur for weakly-ionized airflow.

Thus, after assuming that the inertia change is negligible and that the momentum loss or gain through collisions between charged species is negligible, the momentum equation becomes:

$$\boldsymbol{V}^k = \boldsymbol{V}^\mathrm{n} + s_k\mu_k\left(\boldsymbol{E} + \boldsymbol{V}^k \times \boldsymbol{B}\right) - \frac{\mu_k}{|C_k|N_k}\nabla P_k \tag{7}$$

where s_k is the sign of the charge of the species under consideration (-1 for electrons, +1 for positive ions, -1 for negative ions). Then, after regrouping all $\boldsymbol{V}^k - \boldsymbol{V}^\mathrm{n}$ terms on the LHS the momentum equation in vector form becomes:

$$\boldsymbol{V}^k - \boldsymbol{V}^\mathrm{n} - s_k\mu_k(\boldsymbol{V}^k - \boldsymbol{V}^\mathrm{n}) \times \boldsymbol{B} = s_k\mu_k\left(\boldsymbol{E} + \boldsymbol{V}^\mathrm{n} \times \boldsymbol{B}\right) - \frac{\mu_k}{|C_k|N_k}\nabla P_k \tag{8}$$

The latter can be readily recast in matrix form as:

$$\begin{bmatrix} 1 & -s_k\mu_k\boldsymbol{B}_3 & s_k\mu_k\boldsymbol{B}_2 \\ s_k\mu_k\boldsymbol{B}_3 & 1 & -s_k\mu_k\boldsymbol{B}_1 \\ -s_k\mu_k\boldsymbol{B}_2 & s_k\mu_k\boldsymbol{B}_1 & 1 \end{bmatrix}\begin{bmatrix} (\boldsymbol{V}^k - \boldsymbol{V}^\mathrm{n})_1 \\ (\boldsymbol{V}^k - \boldsymbol{V}^\mathrm{n})_2 \\ (\boldsymbol{V}^k - \boldsymbol{V}^\mathrm{n})_3 \end{bmatrix} = s_k\mu_k\begin{bmatrix} (\boldsymbol{E} + \boldsymbol{V}^\mathrm{n} \times \boldsymbol{B})_1 \\ (\boldsymbol{E} + \boldsymbol{V}^\mathrm{n} \times \boldsymbol{B})_2 \\ (\boldsymbol{E} + \boldsymbol{V}^\mathrm{n} \times \boldsymbol{B})_3 \end{bmatrix} - \frac{\mu_k}{|C_k|N_k}\begin{bmatrix} \partial P_k/\partial x_1 \\ \partial P_k/\partial x_2 \\ \partial P_k/\partial x_3 \end{bmatrix} \tag{9}$$

Then, by defining the tensor mobility $\widetilde{\mu}^k$ as:

$$\begin{aligned}\widetilde{\mu}^k &\equiv \mu_k \begin{bmatrix} 1 & -s_k\mu_k \boldsymbol{B}_3 & s_k\mu_k \boldsymbol{B}_2 \\ s_k\mu_k \boldsymbol{B}_3 & 1 & -s_k\mu_k \boldsymbol{B}_1 \\ -s_k\mu_k \boldsymbol{B}_2 & s_k\mu_k \boldsymbol{B}_1 & 1 \end{bmatrix}^{-1} \\ &= \frac{\mu_k}{1+\mu_k^2|\boldsymbol{B}|^2} \begin{bmatrix} 1+\mu_k^2\boldsymbol{B}_1^2 & \mu_k^2\boldsymbol{B}_1\boldsymbol{B}_2 + s_k\mu_k\boldsymbol{B}_3 & \mu_k^2\boldsymbol{B}_1\boldsymbol{B}_3 - s_k\mu_k\boldsymbol{B}_2 \\ \mu_k^2\boldsymbol{B}_1\boldsymbol{B}_2 - s_k\mu_k\boldsymbol{B}_3 & 1+\mu_k^2\boldsymbol{B}_2^2 & \mu_k^2\boldsymbol{B}_2\boldsymbol{B}_3 + s_k\mu_k\boldsymbol{B}_1 \\ \mu_k^2\boldsymbol{B}_1\boldsymbol{B}_3 + s_k\mu_k\boldsymbol{B}_2 & \mu_k^2\boldsymbol{B}_2\boldsymbol{B}_3 - s_k\mu_k\boldsymbol{B}_1 & 1+\mu_k^2\boldsymbol{B}_3^2 \end{bmatrix}\end{aligned} \tag{10}$$

and multiplying all terms in the momentum equation by the tensor mobility and then dividing through my the scalar mobility, we obtain the charged species momentum equation in tensor form:

$$\boldsymbol{V}_i^k = \boldsymbol{V}_i^{\mathrm{n}} + \sum_j s_k \widetilde{\mu}_{ij}^k \left(\boldsymbol{E} + \boldsymbol{V}^{\mathrm{n}} \times \boldsymbol{B}\right)_j - \sum_j \frac{\widetilde{\mu}_{ij}^k}{|C_k|N_k} \frac{\partial P_k}{\partial x_j} \tag{11}$$

It is emphasized that the latter is derived from the inviscid form of the charged species momentum equation by making only two assumptions: (i) the momentum exchange through collisions with other charged species is much less than through collisions with the neutrals, and (ii) the change in inertia is negligible. The latter assumptions have been shown to be generally valid for weakly-ionized airflow problems.

2.2. Charged Species Mass Conservation

Including the chemical reaction rates, the mass conservation equation for the charged species takes on the form:

$$\frac{\partial N_k}{\partial t} + \sum_i \frac{\partial}{\partial x_i}(N_k \boldsymbol{V}_i^k) = W_k \tag{12}$$

where W_k is the chemical reaction source term for the species under consideration. Because the species velocity $\boldsymbol{V}^k$ is here defined as the sum of the drift and the diffusion velocity, the mass conservation equation as outlined in Eq. (12) takes into account diffusion.

Then, multiplying the mass conservation equation by the charge and taking the sum over all species results in:

$$\sum_k C_k \frac{\partial N_k}{\partial t} + \sum_k \sum_i \frac{\partial}{\partial x_i}(C_k N_k \boldsymbol{V}_i^k) = \sum_k C_k W_k \tag{13}$$

It is noted that the RHS of the latter equation is zero since no net charge can be created or destroyed by the chemical processes. Then, the charged species mass conservation equation becomes the conservation of charge equation:

$$\sum_k C_k \frac{\partial N_k}{\partial t} + \sum_k \sum_i \frac{\partial}{\partial x_i}(C_k N_k \boldsymbol{V}_i^k) = 0 \tag{14}$$

3. Generalized Ohm's Law

By using the momentum and mass conservation equations, we here derive the generalized Ohm's law. Consider the current density $\boldsymbol{J}$ defined as the net mass flux of charges:

$$\boldsymbol{J}_i \equiv \sum_k C_k N_k \boldsymbol{V}_i^k \tag{15}$$

where the species velocity $\boldsymbol{V}^k$ includes both drift velocity and diffusion velocity. The charged species velocity at steady-state can be obtained from the momentum equation for each species, Eq. (11):

$$\boldsymbol{V}_i^k = \boldsymbol{V}_i^{\mathrm{n}} + \sum_j s_k \widetilde{\mu}_{ij}^k \left(\boldsymbol{E} + \boldsymbol{V}^{\mathrm{n}} \times \boldsymbol{B}\right)_j - \sum_j \frac{\widetilde{\mu}_{ij}^k}{|C_k|N_k} \frac{\partial P_k}{\partial x_j} \tag{16}$$

It is recalled that the latter form of the momentum equation assumes that the plasma is weakly-ionized. That is, the terms involving changes in inertia and collisions between charged particles can be considered negligible compared to the terms involving electromagnetic forces and collisions between a charged particle and a neutral. Then, after substituting the latter in the former, we obtain the so-called generalized Ohm's law:

$$\boldsymbol{J}_i = \sum_j \sum_k |C_k| N_k \widetilde{\mu}_{ij}^k \left(\boldsymbol{E} + \boldsymbol{V}^{\mathrm{n}} \times \boldsymbol{B}\right)_j - \sum_j \sum_k s_k \widetilde{\mu}_{ij}^k \frac{\partial P_k}{\partial x_j} + \sum_k \boldsymbol{C}_k N_k \boldsymbol{V}_i^{\mathrm{n}} \tag{17}$$

Then, defining the conductivity as:

$$\begin{aligned} \widetilde{\sigma} &\equiv \sum_k |C_k| N_k \widetilde{\mu}^k \\ &= \sum_k \frac{|C_k| N_k \mu_k}{1 + \mu_k^2 |\boldsymbol{B}|^2} \begin{bmatrix} 1 + \mu_k^2 \boldsymbol{B}_1^2 & \mu_k^2 \boldsymbol{B}_1 \boldsymbol{B}_2 + s_k \mu_k \boldsymbol{B}_3 & \mu_k^2 \boldsymbol{B}_1 \boldsymbol{B}_3 - s_k \mu_k \boldsymbol{B}_2 \\ \mu_k^2 \boldsymbol{B}_1 \boldsymbol{B}_2 - s_k \mu_k \boldsymbol{B}_3 & 1 + \mu_k^2 \boldsymbol{B}_2^2 & \mu_k^2 \boldsymbol{B}_2 \boldsymbol{B}_3 + s_k \mu_k \boldsymbol{B}_1 \\ \mu_k^2 \boldsymbol{B}_1 \boldsymbol{B}_3 + s_k \mu_k \boldsymbol{B}_2 & \mu_k^2 \boldsymbol{B}_2 \boldsymbol{B}_3 - s_k \mu_k \boldsymbol{B}_1 & 1 + \mu_k^2 \boldsymbol{B}_3^2 \end{bmatrix} \end{aligned} \tag{18}$$

the generalized Ohm's law simplifies to:

$$\boldsymbol{J}_i = \sum_j \widetilde{\sigma}_{ij} \left(\boldsymbol{E} + \boldsymbol{V}^{\mathrm{n}} \times \boldsymbol{B}\right)_j - \sum_j \sum_k s_k \widetilde{\mu}_{ij}^k \frac{\partial P_k}{\partial x_j} + \sum_k C_k N_k \boldsymbol{V}_i^{\mathrm{n}} \tag{19}$$

Because of the presence of the last term on RHS, the latter can be applied to non-neutral regions of the plasma such as the plasma sheaths. For the special case of a quasi-neutral plasma, the last term on the RHS can be dropped.

It is emphasized that Eq. (19) includes the Hall effect and the ion slip effect. The ion slip includes the separate contributions to the current from each kind of ion. For instance, for a plasma composed of O_2^-, N_2^+, e^-, the effect of the ion slip associated with the O_2^- ion is taken into account as well as the ion slip effect associated with the N_2^+ ion.

3.1. Charge Carriers Limited to Electrons and One Kind of Positive Ions

For a plasma composed of only electrons and one type of positive ions, the tensor conductivity Eq. (18) would become:

$$\widetilde{\sigma} = \frac{\sigma}{\alpha_1 + \alpha_2} \begin{bmatrix} \alpha_2 \widehat{\boldsymbol{B}}_1^2 + \alpha_1 & \alpha_2 \widehat{\boldsymbol{B}}_1 \widehat{\boldsymbol{B}}_2 - \alpha_3 \widehat{\boldsymbol{B}}_3 & \alpha_2 \widehat{\boldsymbol{B}}_1 \widehat{\boldsymbol{B}}_3 + \alpha_3 \widehat{\boldsymbol{B}}_2 \\ \alpha_2 \widehat{\boldsymbol{B}}_1 \widehat{\boldsymbol{B}}_2 + \alpha_3 \widehat{\boldsymbol{B}}_3 & \alpha_2 \widehat{\boldsymbol{B}}_2^2 + \alpha_1 & \alpha_2 \widehat{\boldsymbol{B}}_2 \widehat{\boldsymbol{B}}_3 - \alpha_3 \widehat{\boldsymbol{B}}_1 \\ \alpha_2 \widehat{\boldsymbol{B}}_1 \widehat{\boldsymbol{B}}_3 - \alpha_3 \widehat{\boldsymbol{B}}_2 & \alpha_2 \widehat{\boldsymbol{B}}_2 \widehat{\boldsymbol{B}}_3 + \alpha_3 \widehat{\boldsymbol{B}}_1 & \alpha_2 \widehat{\boldsymbol{B}}_3^2 + \alpha_1 \end{bmatrix} \tag{20}$$

In the latter, the normalized magnetic field is defined as $\widehat{\boldsymbol{B}}_i \equiv \boldsymbol{B}_i / |\boldsymbol{B}|$, while the Hall parameter for the electrons and ions is defined as $\beta_{\mathrm{e}} \equiv \mu_{\mathrm{e}} |\boldsymbol{B}|$ and $\beta_{\mathrm{i}} \equiv \mu_{\mathrm{i}} |\boldsymbol{B}|$ respectively. The conductivity includes a contribution from the ions and the electrons, i.e. $\sigma = |C_{\mathrm{i}}| N_{\mathrm{i}} \mu_{\mathrm{i}} + |C_{\mathrm{e}}| N_{\mathrm{e}} \mu_{\mathrm{e}}$, and the parameters α_1, α_2, and α_3 correspond to:

$$\alpha_1 = 1 + \beta_{\mathrm{e}} \beta_{\mathrm{i}} \tag{21}$$

$$\alpha_2 = (\beta_{\mathrm{e}} - \beta_{\mathrm{i}})^2 + \beta_{\mathrm{e}} \beta_{\mathrm{i}} + (\beta_{\mathrm{e}} \beta_{\mathrm{i}})^2 \tag{22}$$

$$\alpha_3 = \beta_{\mathrm{e}} - \beta_{\mathrm{i}} \tag{23}$$

In tensor form, the generalized Ohm's law has the same formulation as Eq. (19). However, in this case (i.e. for a plasma in which current is carried only by one kind of positive ions and by electrons), the generalized Ohm's law can also be written in vector form. Indeed, for the conductivity outlined in Eq. (20), it can be shown that, should the pressure gradients and non-neutral terms be neglected, the generalized Ohm's law outlined in Eq. (19) becomes exactly:

$$\boldsymbol{J} = \sigma(\boldsymbol{E} + \boldsymbol{V}^{\mathrm{n}} \times \boldsymbol{B}) + \frac{\beta_{\mathrm{i}}}{|\boldsymbol{B}|} \boldsymbol{J} \times \boldsymbol{B} - \frac{\beta_{\mathrm{e}}}{|\boldsymbol{B}|} \boldsymbol{J} \times \boldsymbol{B} + \frac{\beta_{\mathrm{e}} \beta_{\mathrm{i}}}{|\boldsymbol{B}|^2} (\boldsymbol{J} \times \boldsymbol{B}) \times \boldsymbol{B} \tag{24}$$

Since the ion mobility is much less than the electron mobility, we can say that $\beta_{\mathrm{i}} \ll \beta_{\mathrm{e}}$. Then the latter becomes the well-known generalized Ohm's law for a quasi-neutral plasma (including ion slip but excluding the pressure gradients):

$$\boldsymbol{J} = \sigma(\boldsymbol{E} + \boldsymbol{V}^{\mathrm{n}} \times \boldsymbol{B}) - \frac{\beta_{\mathrm{e}}}{|\boldsymbol{B}|}\boldsymbol{J} \times \boldsymbol{B} + \frac{\beta_{\mathrm{e}}\beta_{\mathrm{i}}}{|\boldsymbol{B}|^2}(\boldsymbol{J} \times \boldsymbol{B}) \times \boldsymbol{B} \tag{25}$$

On the RHS, the first term gives the effect of the electric field, the second term is the Hall effect and the last term is the ion slip [14, 19].

3.2. Charge Carriers Limited to Electrons

The tensor conductivity [Eq. (18)] can be further simplified for the case of a plasma in which the current is only carried by the electrons (that is, neglecting the effect of ion slip):

$$\widetilde{\sigma} = \frac{\sigma}{1+\beta_{\mathrm{e}}^2}\begin{bmatrix} \beta_{\mathrm{e}}^2\widehat{\boldsymbol{B}}_1^2 + 1 & \beta_{\mathrm{e}}^2\widehat{\boldsymbol{B}}_1\widehat{\boldsymbol{B}}_2 - \beta_{\mathrm{e}}\widehat{\boldsymbol{B}}_3 & \beta_{\mathrm{e}}^2\widehat{\boldsymbol{B}}_1\widehat{\boldsymbol{B}}_3 + \beta_{\mathrm{e}}\widehat{\boldsymbol{B}}_2 \\ \beta_{\mathrm{e}}^2\widehat{\boldsymbol{B}}_1\widehat{\boldsymbol{B}}_2 + \beta_{\mathrm{e}}\widehat{\boldsymbol{B}}_3 & \beta_{\mathrm{e}}^2\widehat{\boldsymbol{B}}_2^2 + 1 & \beta_{\mathrm{e}}^2\widehat{\boldsymbol{B}}_2\widehat{\boldsymbol{B}}_3 - \beta_{\mathrm{e}}\widehat{\boldsymbol{B}}_1 \\ \beta_{\mathrm{e}}^2\widehat{\boldsymbol{B}}_1\widehat{\boldsymbol{B}}_3 - \beta_{\mathrm{e}}\widehat{\boldsymbol{B}}_2 & \beta_{\mathrm{e}}^2\widehat{\boldsymbol{B}}_2\widehat{\boldsymbol{B}}_3 + \beta_{\mathrm{e}}\widehat{\boldsymbol{B}}_1 & \beta_{\mathrm{e}}^2\widehat{\boldsymbol{B}}_3^2 + 1 \end{bmatrix} \tag{26}$$

where the normalized magnetic field vector $\widehat{\boldsymbol{B}}$ is defined as $\boldsymbol{B}/|\boldsymbol{B}|$, where the conductivity σ corresponds to $|C_{\mathrm{e}}|N_{\mathrm{e}}\mu_{\mathrm{e}}$ and where the Hall parameter β_{e} is equal to $\mu_{\mathrm{e}}|\boldsymbol{B}|$. In tensor form, the generalized Ohm's law can be written as a function of the tensor conductivity as in Eq. (19). However, when the tensor conductivity is as described in Eq. (26) and when non-neutral and pressure gradient effects are neglected, the generalized Ohm's law outlined in Eq. (19) collapses exactly to:

$$\boldsymbol{J} = \sigma(\boldsymbol{E} + \boldsymbol{V}^{\mathrm{n}} \times \boldsymbol{B}) - \frac{\beta_{\mathrm{e}}}{|\boldsymbol{B}|}\boldsymbol{J} \times \boldsymbol{B} \tag{27}$$

On the RHS, the first term gives the effect of the electric field, and the second term is the Hall effect [14].

4. Electric Field Potential Equation

By substituting the current defined in Eq. (15) into the mass conservation equation previously outlined in Eq. (14), it can be shown that the divergence of the current density is equal to the negative rate of change of the charge density:

$$\sum_i \frac{\partial}{\partial x_i}\boldsymbol{J}_i = -\sum_k C_k \frac{\partial N_k}{\partial t} \tag{28}$$

Then, recall that under the assumption of negligible inertia change, negligible shear stress, and negligible momentum loss through collisions between charged particles, we obtained an expression for the current in Eq. (19) which we referred to as the generalized Ohm's law:

$$\boldsymbol{J}_i = \sum_j \widetilde{\sigma}_{ij}\left(\boldsymbol{E} + \boldsymbol{V}^{\mathrm{n}} \times \boldsymbol{B}\right)_j - \sum_j \sum_k s_k \widetilde{\mu}_{ij}^k \frac{\partial P_k}{\partial x_j} + \sum_k C_k N_k \boldsymbol{V}_i^{\mathrm{n}} \tag{29}$$

Substituting the latter in the former yields:

$$\sum_i \frac{\partial}{\partial x_i}\left(\sum_j \widetilde{\sigma}_{ij}\left(\boldsymbol{E} + \boldsymbol{V}^{\mathrm{n}} \times \boldsymbol{B}\right)_j - \sum_j \sum_k s_k \widetilde{\mu}_{ij}^k \frac{\partial P_k}{\partial x_j} + \sum_k C_k N_k \boldsymbol{V}_i^{\mathrm{n}}\right) = -\sum_k C_k \frac{\partial N_k}{\partial t} \tag{30}$$

Let's now assume that a potential of the electric field exists, such that:

$$\boldsymbol{E}_j = -\frac{\partial \phi}{\partial x_j} \tag{31}$$

The existence of a potential for the electric field implies that the curl of the electric field is zero. For the curl of the electric field to be zero, the magnetic field can not vary in time. This is a reasonable assumption for weakly-ionized flowfields as long as the external magnetic field does not vary in time. Indeed, the induced magnetic field can be considered negligible for weakly-ionized plasmas because the latter exhibit a low magnetic Reynolds number.

Then, substituting $\boldsymbol{E}_j = -\partial\phi/\partial x_j$ in the current conservation equation, the electric field potential equation is obtained:

$$\sum_i \frac{\partial}{\partial x_i}\left(\sum_j \widetilde{\sigma}_{ij}\left(-\frac{\partial\phi}{\partial x_j} + (\boldsymbol{V}^{\mathrm{n}}\times\boldsymbol{B})_j\right) - \sum_j\sum_k s_k\widetilde{\mu}^k_{ij}\frac{\partial P_k}{\partial x_j} + \sum_k C_k N_k \boldsymbol{V}^{\mathrm{n}}_i\right) = -\sum_k C_k\frac{\partial N_k}{\partial t} \tag{32}$$

We can simplify the latter by regrouping the terms that are not directly a function of the potential in the source term S:

$$S = -\sum_i \frac{\partial}{\partial x_i}\sum_j \widetilde{\sigma}_{ij}\,(\boldsymbol{V}^{\mathrm{n}}\times\boldsymbol{B})_j + \sum_i\frac{\partial}{\partial x_i}\sum_j\sum_k s_k\widetilde{\mu}^k_{ij}\frac{\partial P_k}{\partial x_j} - \sum_i\frac{\partial}{\partial x_i}\sum_k C_k N_k\boldsymbol{V}^{\mathrm{n}}_i - \sum_k C_k\frac{\partial N_k}{\partial t} \tag{33}$$

Then, the potential equation collapses to the following much simpler expression:

$$\sum_i \frac{\partial}{\partial x_i}\sum_j \widetilde{\sigma}_{ij}\left(-\frac{\partial\phi}{\partial x_j}\right) = S \tag{34}$$

It is emphasized that the latter includes the effect of non-neutrality, the effect of the ion and electron pressure gradients, the effect of mass diffusion, the Hall effect, as well as the effect of ion slip for each type of ion. For instance, for a plasma made of electrons, N_2^+, O_2^-, O_2^+, etc, *the current due to ion slip of each ion type is taken into consideration*.

4.1. Recast of the Potential Equation in a Form Amenable to Discretization

Equation (34) seems to be a Poisson-like equation consisting of only diffusion and source terms. It is well known that diffusion terms can be successfully discretized using central differences without introducing spurious oscillations. However, as will be shown in this section, the potential equation outlined in Eq. (34) is not strictly a Poisson equation because some of the cross-diffusion terms can be rewritten as convection derivatives. Then, contrarily to the Poisson equation, the potential equation cannot be discretized by only using central differences due to the presence of convection terms. It is hence important at this stage to rewrite some of the diffusion terms as convection derivatives in order to obtain an expression for the potential equation that is amenable to discretization.

For this matter, let's rewrite the tensorial conductivity as a sum of a symmetric matrix and a skew-symmetric matrix:

$$\widetilde{\sigma} = \widetilde{\sigma}^{\mathrm{S}} + \widetilde{\sigma}^{\mathrm{SS}} \tag{35}$$

with the symmetric matrix equal to:

$$\widetilde{\sigma}^{\mathrm{S}} = \sum_k \frac{|C_k|N_k\mu_k}{1+\mu_k^2|\boldsymbol{B}|^2}\begin{bmatrix} 1+\mu_k^2\boldsymbol{B}_1^2 & \mu_k^2\boldsymbol{B}_1\boldsymbol{B}_2 & \mu_k^2\boldsymbol{B}_1\boldsymbol{B}_3 \\ \mu_k^2\boldsymbol{B}_1\boldsymbol{B}_2 & 1+\mu_k^2\boldsymbol{B}_2^2 & \mu_k^2\boldsymbol{B}_2\boldsymbol{B}_3 \\ \mu_k^2\boldsymbol{B}_1\boldsymbol{B}_3 & \mu_k^2\boldsymbol{B}_2\boldsymbol{B}_3 & 1+\mu_k^2\boldsymbol{B}_3^2 \end{bmatrix} \tag{36}$$

and the skew-symmetric matrix equal to:

$$\widetilde{\sigma}^{\mathrm{SS}} = \sum_k \frac{|C_k|N_k\mu_k}{1+\mu_k^2|\boldsymbol{B}|^2}\begin{bmatrix} 0 & s_k\mu_k\boldsymbol{B}_3 & -s_k\mu_k\boldsymbol{B}_2 \\ -s_k\mu_k\boldsymbol{B}_3 & 0 & s_k\mu_k\boldsymbol{B}_1 \\ s_k\mu_k\boldsymbol{B}_2 & -s_k\mu_k\boldsymbol{B}_1 & 0 \end{bmatrix} \tag{37}$$

Then, after substituting the latter in the electric field potential equation, the following is obtained:

$$-\sum_i\frac{\partial}{\partial x_i}\sum_j\widetilde{\sigma}^{\mathrm{S}}_{ij}\frac{\partial\phi}{\partial x_j} - \sum_i\frac{\partial}{\partial x_i}\sum_j\widetilde{\sigma}^{\mathrm{SS}}_{ij}\frac{\partial\phi}{\partial x_j} = S \tag{38}$$

It can be easily shown that the term function of the skew-symmetric conductivity tensor can be rewritten to:

$$\sum_i\frac{\partial}{\partial x_i}\sum_j\widetilde{\sigma}^{\mathrm{SS}}_{ij}\frac{\partial\phi}{\partial x_j} = \sum_i\sum_j\frac{\partial}{\partial x_j}\left(\frac{\partial\widetilde{\sigma}^{\mathrm{SS}}_{ij}}{\partial x_i}\phi\right) - \phi\sum_i\sum_j\frac{\partial^2\widetilde{\sigma}^{\mathrm{SS}}_{ij}}{\partial x_i\partial x_j} + \sum_i\sum_j\widetilde{\sigma}^{\mathrm{SS}}_{ij}\frac{\partial^2\phi}{\partial x_j\partial x_i} \tag{39}$$

The last two terms on the RHS will always be zero due to the commutativity of differentiation and due to the matrix $\widetilde{\sigma}^{\mathrm{SS}}$ being skew-symmetric and having diagonal elements equal to zero. Then, the electric field potential equation collapses to:

$$-\sum_i \frac{\partial}{\partial x_i} \sum_j \widetilde{\sigma}^{\mathrm{S}}_{ij} \frac{\partial \phi}{\partial x_j} - \sum_i \sum_j \frac{\partial}{\partial x_j} \left(\frac{\partial \widetilde{\sigma}^{\mathrm{SS}}_{ij}}{\partial x_i} \phi \right) = S \tag{40}$$

By substituting the i and j indices of the term function of the skew-symmetric conductivity and defining the wave speed associated with the skew-symmetric terms as

$$a^{\mathrm{SS}}_i \equiv -\sum_j \frac{\partial \widetilde{\sigma}^{\mathrm{SS}}_{ji}}{\partial x_j} \tag{41}$$

the potential equation becomes:

$$\sum_i \frac{\partial}{\partial x_i} a^{\mathrm{SS}}_i \phi - \sum_i \frac{\partial}{\partial x_i} \sum_j \widetilde{\sigma}^{\mathrm{S}}_{ij} \frac{\partial \phi}{\partial x_j} = S \tag{42}$$

Rather interestingly, the skew-symmetric diffusion terms can be seen to collapse to a convection-like derivative, with the wave speed being proportional to the gradient of the conductivity. When written in this form, the electric field potential equation is hence seen not to be strictly a diffusion equation. Rather, it includes a first order derivative additionally to the second order derivative.

It is noted that the first order derivative does not always affect appreciably the solution. Indeed, the first-order derivative becomes significant only in the *simultaneous* presence of a high Hall parameter and a high gradient of the electrical conductivity. While not necessarily a common occurrence in weakly-ionized flowfields, such a high Hall parameter combined with a strong conductivity gradient has been observed in Faraday generators and accelerators using e-beam-ionized airflow as the working fluid (see Ref. [11] for instance).

5. Discretization of the Potential Equation

Having expressed the potential equation in a form amenable to discretization by rewriting the skew-symmetric diffusion derivatives as convection derivatives, we can now proceed to its discretization. In discrete form, the potential equation outlined in Eq. (42) can be expressed as:

$$\sum_i \delta_{x_i} \left(a^{\mathrm{SS}}_i \phi \right) - \sum_i \delta_{x_i} \sum_j \left(\widetilde{\sigma}^{\mathrm{S}}_{ij} \delta_{x_j} \phi \right) = S_\Delta \tag{43}$$

Because central differences cannot be used to discretize a convection derivative without introducing even-odd discoupling of the properties, it is necessary to use an upwinded stencil to discretize the first derivative to prevent spurious oscillations from forming. Therefore, in conservative form on a uniformly-spaced mesh, the discretization stencil of the skew-symmetric terms is set to:

$$\left[\delta_{x_i} \left(a^{\mathrm{SS}}_i \phi \right) \right]^{X_i} = \frac{\left(a^{\mathrm{SS}}_i \phi \right)^{X_i + \frac{1}{2}} - \left(a^{\mathrm{SS}}_i \phi \right)^{X_i - \frac{1}{2}}}{\Delta x_i} \tag{44}$$

where Δx_i refers to the grid spacing (which is here assumed constant for simplicity) and where X_i refers to the grid index. For instance, the notation $(X_1 = 10,\ X_2 = 5)$ refers to the node $(10,\ 5)$. The flux at the interface is discretized using an upwinded stencil combined with a symmetric minmod TVD limiter [20]:

$$\left(a^{\mathrm{SS}}_i \phi \right)^{X_i + \frac{1}{2}} = \frac{1}{2} \left(a^{\mathrm{SS}}_i \phi \right)^{X_i} + \frac{1}{2} \left(a^{\mathrm{SS}}_i \phi \right)^{X_i + 1} - \frac{1}{2} \left| a^{\mathrm{SS}}_i \right|^{X_i + \frac{1}{2}} \Delta \phi^{X_i + \frac{1}{2}} + \frac{1}{2} \left| a^{\mathrm{SS}}_i \right|^{X_i + \frac{1}{2}} \ \mathrm{minmod} \left(\Delta \phi^{X_i - \frac{1}{2}},\ \Delta \phi^{X_i + \frac{1}{2}},\ \Delta \phi^{X_i + \frac{3}{2}} \right) \tag{45}$$

with $\Delta \phi^{X_i + \frac{1}{2}} \equiv \phi^{X_i + 1} - \phi^{X_i}$ and where the minmod function returns the minimum of its arguments if the arguments are all positive, the maximum if the arguments are all negative, and zero if the arguments are of mixed signs. Such a stencil is monotonicity-preserving while being second-order accurate in regions where the properties vary smoothly. The other diffusion terms can be discretized with centered stencils as they do not pose any problem:

$$\left[\delta_{x_i} \left(\widetilde{\sigma}^{\mathrm{S}}_{ij} \delta_{x_j} \phi \right) \right]^{X_i} = \frac{\left(\widetilde{\sigma}^{\mathrm{S}}_{ij} \delta_{x_j} \phi \right)^{X_i + \frac{1}{2}} - \left(\widetilde{\sigma}^{\mathrm{S}}_{ij} \delta_{x_j} \phi \right)^{X_i - \frac{1}{2}}}{\Delta x_i} \tag{46}$$

where the flux at the interface would correspond to, when $i = j$:

$$\left(\widetilde{\sigma}^{\mathrm{S}}_{ij}\delta_{x_j}\phi\right)^{X_i+\frac{1}{2}} = \left(\widetilde{\sigma}^{\mathrm{S}}_{ii}\right)^{X_i+\frac{1}{2}} \frac{\phi^{X_i+1} - \phi^{X_i}}{\Delta x_i} \tag{47}$$

and to, when $i \neq j$:

$$\left(\widetilde{\sigma}^{\mathrm{S}}_{ij}\delta_{x_j}\phi\right)^{X_i+\frac{1}{2}} = \left(\widetilde{\sigma}^{\mathrm{S}}_{ij}\right)^{X_i+\frac{1}{2},X_j} \times \frac{\phi^{X_i,X_j+1} + \phi^{X_i+1,X_j+1} - \phi^{X_i,X_j-1} - \phi^{X_i+1,X_j-1}}{4\Delta x_j} \tag{48}$$

6. Pseudotime Relaxation of the Discrete Potential Equation

The solution of the potential equation can be accomplished efficiently through an implicit pseudotime relaxation algorithm. The algorithm consists of adding a pseudotime derivative to the potential equation, and rewriting the latter in delta form:

$$\frac{\Delta^n\phi}{\Delta\tau} + \sum_i \delta_{x_i}\Delta^n\left(\left(a^{\mathrm{SS}}_i\phi\right) - \sum_j\left(\widetilde{\sigma}^{\mathrm{S}}_{ij}\delta_{x_j}\phi\right)\right) - \Delta^n S = -R^n_\Delta \tag{49}$$

with $\Delta^n() \equiv ()^{n+1} - ()^n$, and where the superscript "n" denotes the pseudotime level. As well, $\Delta\tau$ corresponds to the pseudotime step. In the latter, the discrete residual corresponds to:

$$R^n_\Delta = \sum_i \delta_{x_i}\left(\left(a^{\mathrm{SS}}_i\phi\right)^n - \sum_j\left(\widetilde{\sigma}^{\mathrm{S}}_{ij}\delta_{x_j}\phi\right)^n\right) - S^n_\Delta \tag{50}$$

Because solving the delta form exactly would require excessive computing effort in 2D or 3D, it is here preferred to solve the delta form approximately through an approximate factorization algorithm [21]. Assuming that the tensor conductivity $\widetilde{\sigma}_{ij}$ and the source term S remain frozen during the integration in pseudotime from time level n to time level $n+1$, the equation to solve at each node for the ith sweep can be shown to correspond to:

$$\begin{aligned}
&-\left(\frac{\widetilde{\sigma}^{X_i-\frac{1}{2}}_{ii}}{\Delta x_i^2} + \frac{(a^{\mathrm{SS}}_i)^{X_i-1} + |a^{\mathrm{SS}}_i|^{X_i-\frac{1}{2}}}{2\Delta x_i}\right)\Delta\phi_i^{X_i-1} + \left(\frac{1}{\Delta\tau^{X_i}} + \left(\frac{\widetilde{\sigma}_{ii}}{\Delta x_i^2} + \frac{|a^{\mathrm{SS}}_i|}{\Delta x_i}\right)^{X_i-\frac{1}{2}} + \left(\frac{\widetilde{\sigma}_{ii}}{\Delta x_i^2} + \frac{|a^{\mathrm{SS}}_i|}{\Delta x_i}\right)^{X_i+\frac{1}{2}}\right)\Delta\phi_i^{X_i} \\
&\quad -\left(\frac{\widetilde{\sigma}^{X_i+\frac{1}{2}}_{ii}}{\Delta x_i^2} + \frac{-(a^{\mathrm{SS}}_i)^{X_i+1} + |a^{\mathrm{SS}}_i|^{X_i+\frac{1}{2}}}{2\Delta x_i}\right)\Delta\phi_i^{X_i+1} = \mathrm{RHS}
\end{aligned} \tag{51}$$

For the first i-sweep (i.e., the sweep along the first dimension), the RHS is set to the negative of the discrete residual at the previous pseudotime level. That is,

$$\mathrm{RHS} = -(R^n_\Delta)^{X_i} \quad \text{for the first sweep.} \tag{52}$$

For the subsequent sweeps, the RHS is set to the potential increment obtained at the previous sweep divided by the pseudotime step. That is,

$$\mathrm{RHS} = \frac{\Delta\phi^{X_i}_{i-1}}{\Delta\tau^{X_i}} \quad \text{for the second and third sweep.} \tag{53}$$

After the sweeps along all dimensions are completed, the potential increment obtained in the last i-sweep is used to find the potential at the next pseudotime level: $\phi^{n+1} = \phi^n + \Delta\phi_d$.

Because the success of approximate factorization relies on the degree of invariance of the linearization coefficients, it is preferred not to include a linearized form of the minmod limiter on the LHS. Not only would this result in additional work to solve a pentadiagonal matrix instead of a tridiagonal one, but this would also induce erratic patterns in the convergence history sometimes even preventing a converged solution altogether.

The convergence rate of the approximate factorization algorithm can be further improved by not fixing the pseudotime step to the same value for all nodes. Rather, it is found (through a trial-and-error approach) that convergence can be reached more

rapidly by allowing the pseudotime step to vary at each node according to the following relationship:

$$\Delta\tau = \xi \times \min_{i=1}^{d} \left(\frac{\Delta x_i}{\max\left(\widetilde{\sigma}_{ii}^{X_i-1},\ \widetilde{\sigma}_{ii}^{X_i},\ \widetilde{\sigma}_{ii}^{X_i+1}\right)} \right) \tag{54}$$

where ξ is a user-defined parameter which is set to 0.07 m for all cases shown herein. The rate of convergence can be further improved by varying the pseudotime step cyclically. For instance, for iteration n, $n+1$, $n+2$, etc, ξ is set to 0.02 m, 0.08 m, 0.32 m, 0.02 m, 0.08 m, etc. Although not used to solve the test cases shown herein, such a cyclic variation of the pseudotime step can be particularly beneficial when solving problems with large variations of the magnetic field or of the grid spacing.

(a) Test Case 1:

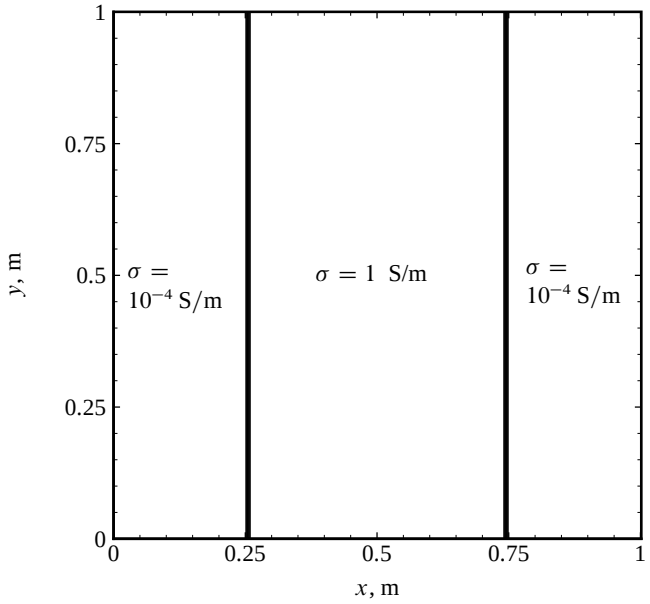

(b) Test Case 2:

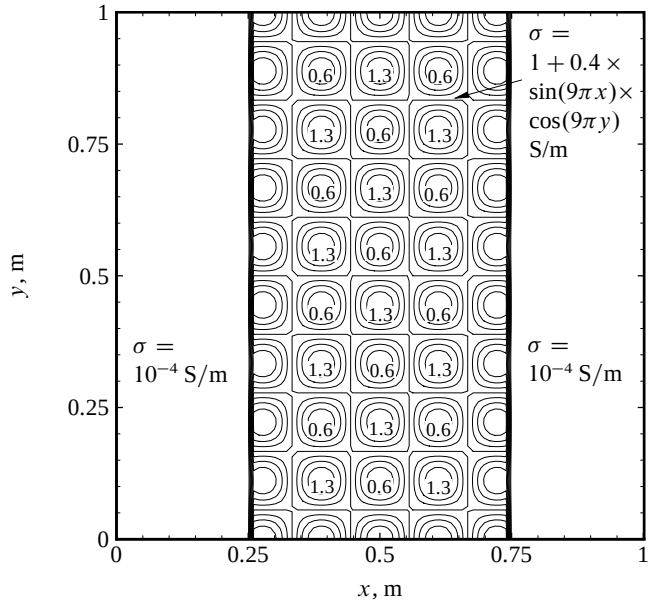

FIGURE 1: Contour levels of the scalar conductivity σ.

7. Test Cases

While the electric field potential equation and its discretization stencil outlined herein are written in general form and can be applied to plasmas in which both electrons and ions can carry current, the test cases here presented are limited for ease of reproducibility to a plasma in which the current is carried solely by the electrons. Also for ease of reproducibility, the source term S is set to zero (that is, the terms related to pressure gradients and non-neutral effects are set to zero). Then, the symmetric conductivity matrix simplifies to:

$$\widetilde{\sigma}^{\mathrm{S}} \rightarrow \frac{\sigma}{1+\beta_{\mathrm{e}}^2} \begin{bmatrix} 1+\beta_{\mathrm{e}}^2\widehat{\boldsymbol{B}}_1^2 & \beta_{\mathrm{e}}^2\widehat{\boldsymbol{B}}_1\widehat{\boldsymbol{B}}_2 & \beta_{\mathrm{e}}^2\widehat{\boldsymbol{B}}_1\widehat{\boldsymbol{B}}_3 \\ \beta_{\mathrm{e}}^2\widehat{\boldsymbol{B}}_1\widehat{\boldsymbol{B}}_2 & 1+\beta_{\mathrm{e}}^2\widehat{\boldsymbol{B}}_2^2 & \beta_{\mathrm{e}}^2\widehat{\boldsymbol{B}}_2\widehat{\boldsymbol{B}}_3 \\ \beta_{\mathrm{e}}^2\widehat{\boldsymbol{B}}_1\widehat{\boldsymbol{B}}_3 & \beta_{\mathrm{e}}^2\widehat{\boldsymbol{B}}_2\widehat{\boldsymbol{B}}_3 & 1+\beta_{\mathrm{e}}^2\widehat{\boldsymbol{B}}_3^2 \end{bmatrix} \tag{55}$$

and the skew-symmetric matrix becomes:

$$\widetilde{\sigma}^{\mathrm{SS}} \rightarrow \frac{\sigma}{1+\beta_{\mathrm{e}}^2} \begin{bmatrix} 0 & -\beta_{\mathrm{e}}\widehat{\boldsymbol{B}}_3 & \beta_{\mathrm{e}}\widehat{\boldsymbol{B}}_2 \\ \beta_{\mathrm{e}}\widehat{\boldsymbol{B}}_3 & 0 & -\beta_{\mathrm{e}}\widehat{\boldsymbol{B}}_1 \\ -\beta_{\mathrm{e}}\widehat{\boldsymbol{B}}_2 & \beta_{\mathrm{e}}\widehat{\boldsymbol{B}}_1 & 0 \end{bmatrix} \tag{56}$$

From the latter, it is apparent that the skew symmetric terms are negligible when the Hall parameter is much less than unity. Additionally, as was shown previously, the skew symmetric terms collapse to zero when there is no gradient of the conductivity. Therefore, in order to test adequately the proposed discretization scheme, the Hall parameter and the conductivity gradient are here set sufficiently high that the skew-symmetric terms predominate over the symmetric terms.

Two test cases are here considered. Both consist of a two-dimensional domain with the following Dirichlet boundary conditions:

$$\phi_{x=0} = 20\ \mathrm{V},\ \ \phi_{x=1\,\mathrm{m}} = 20\ \mathrm{V},\ \ \phi_{y=0} = 10\ \mathrm{V},\ \ \phi_{y=1\,\mathrm{m}} = 40\ \mathrm{V} \tag{57}$$

with the Hall parameter fixed to 20, and the bulk gas velocity fixed to zero. For test case 1, the conductivity is such that it exhibits a strong gradient in some regions of the domain to test the monotonicity-preserving capabilities of the discretization

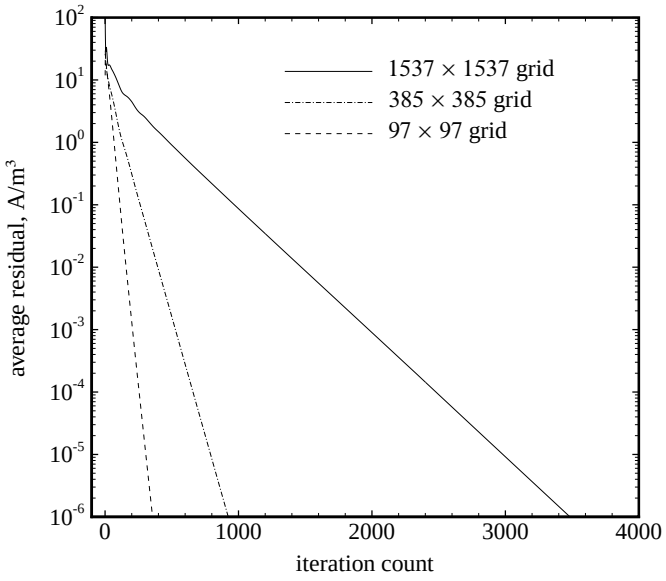

FIGURE 2: Average residual error as a function of the iteration count for the second test case using the proposed upwinded scheme.

(a) Standard 9-point central-difference stencil

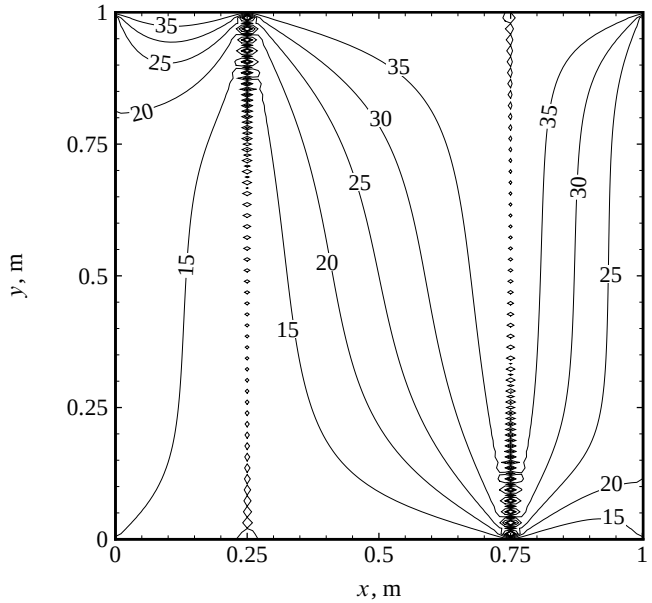

(b) Proposed 13-point upwinded stencil

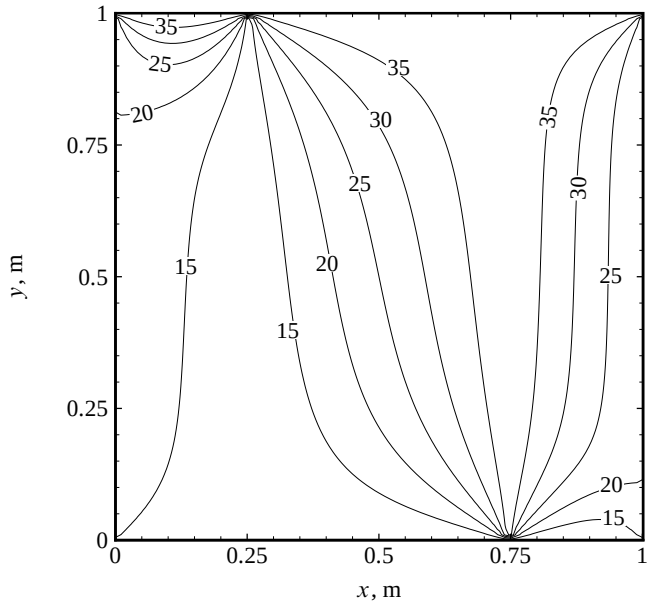

FIGURE 3: Potential contours (in volts) for the first test case using a 97×97 grid.

scheme (see Fig. 1a):

$$\sigma = \begin{cases} 1.0 \text{ S/m} & \text{for } 0.25 \text{ m} \leq x \leq 0.75 \text{ m} \\ 0.0001 \text{ S/m} & \text{otherwise} \end{cases} \tag{58}$$

For test case 2, the conductivity is given a variation in the central portion of the domain to test the order of accuracy of the scheme in smoothly-varying regions (see Fig. 1b):

$$\sigma = \begin{cases} 1.0 + 0.4 \times \sin(9\pi x) \times \cos(9\pi y) \text{ S/m} & \text{for } 0.25 \text{ m} \leq x \leq 0.75 \text{ m} \\ 0.0001 \text{ S/m} & \text{otherwise} \end{cases} \tag{59}$$

(a) Standard 9-point central-difference stencil

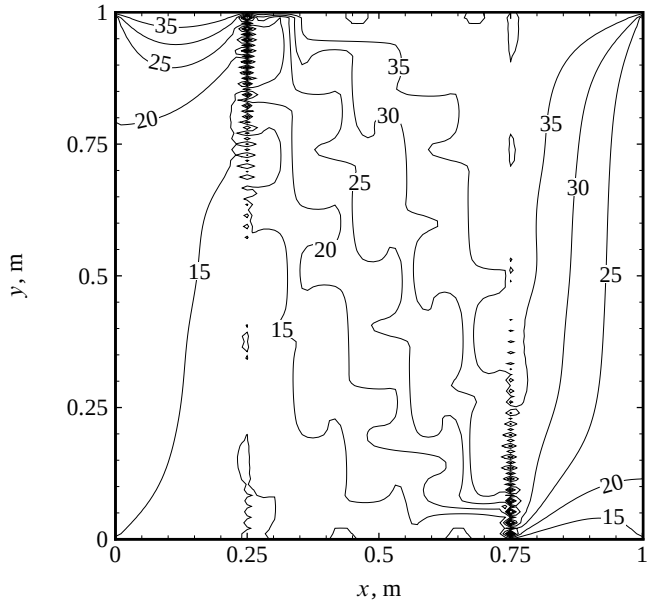

(b) Proposed 13-point upwinded stencil

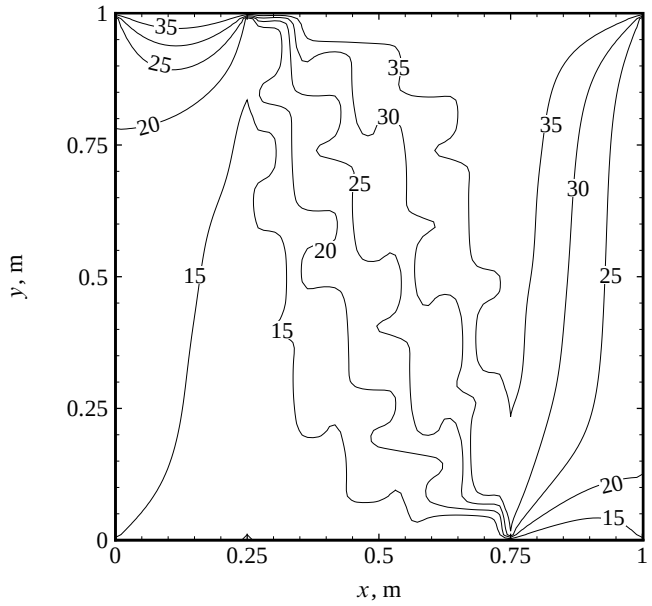

FIGURE 4: Potential contours (in volts) for the second test case using a 97×97 grid.

Even thus the gradient of the conductivity is high and the Hall parameter is high, spurious oscillations may still not occur. Indeed, the skew-symmetric terms may become negligible for certain orientations of the magnetic field vector. It can be easily shown that this would occur when the magnetic field vector lies within the plane made by the potential gradient vector and the conductivity gradient vector. For this reason and because it is desired to test the monotonicity-preserving capability of the proposed scheme under the most stringent conditions, the normalized magnetic field vector is here fixed perpendicular to the computational domain:

$$\widehat{\boldsymbol{B}} = (0,\ 0,\ 1) \tag{60}$$

It is noted that the magnitude of the magnetic field is not specified. Indeed, it is not necessary to specify the magnitude of the magnetic field because it does not appear explicitly in the simplified potential equation used in this section. Rather, the potential

(a) $\boldsymbol{E}_x$ at $y = 0.5$ m

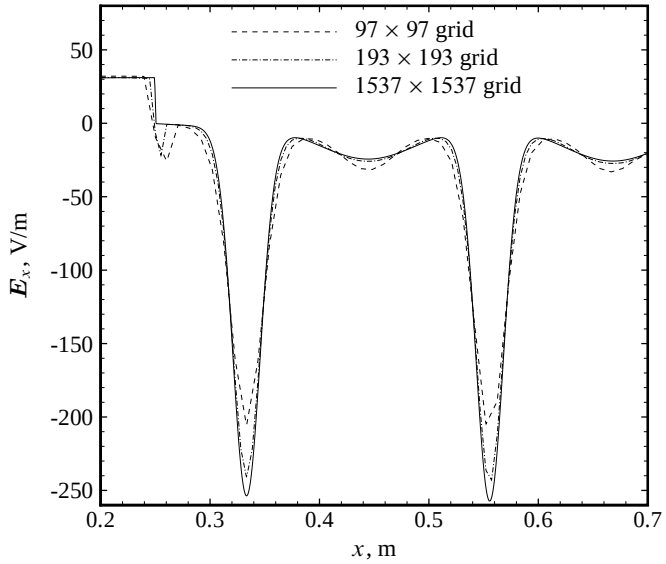

(b) $\boldsymbol{E}_y$ at $y = 0.5$ m

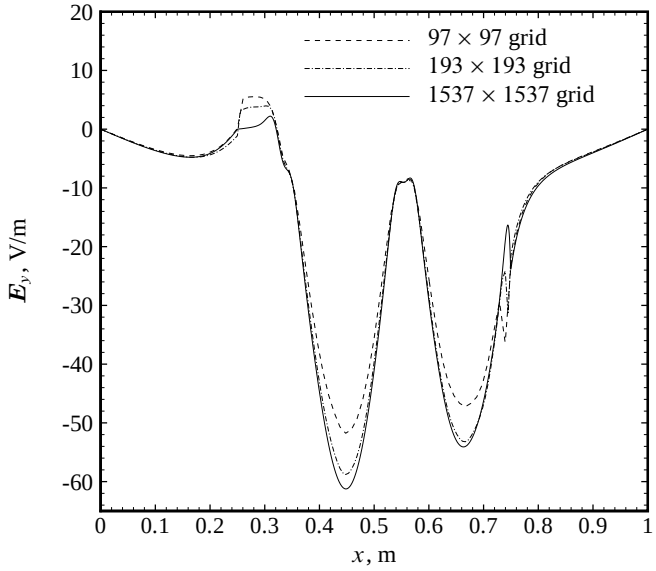

FIGURE 5: Grid convergence study of the electric field for the second test case using the proposed upwinded scheme.

equation is written in terms of the Hall parameter.

For all cases here presented, the solution is obtained through the use of pseudotime relaxation. That is, the solution is advanced in pseudotime through the use of an implicit approximate factorization algorithm until convergence is attained. The solution is considered converged when the discrete residual on all nodes falls below a threshold set to 10^{-4}. This is verified to be sufficiently small to yield potential contours that are visually indistinguishable from those obtained using a residual convergence threshold set to machine tolerance (about 10^{-13}). The variation of the average residual as a function of the iteration count is shown for the second test case in Fig. 2. The approximate factorization scheme is seen to yield a reasonably fast convergence rate, with a converged solution being obtained in less than 300 iterations for the coarsest mesh. The number of iterations necessary to reach convergence can be observed to vary inversely proportionally with the grid spacing. This is as anticipated because the pseudotime step [as defined previously in Eq. (54)] is proportional to the mesh spacing and the amount

of pseudotime necessary to reach convergence is more or less independent of the mesh size.

A comparison between the potential contours obtained with the standard 9-point central-difference stencil and the proposed 13-point upwinded stencil is performed for the first test case (see Fig. 3). As expected, the use of the standard central-difference stencil is seen to introduce severe spurious oscillations of the electric field potential in the regions where the gradient of the conductivity is high. Such aphysical oscillations of the potential are completely removed when the upwinded stencil is used. A similar conclusion can be reached for the second test case: as shown in Fig. 4, the central-difference stencil introduces spurious oscillations in the regions where a discontinuity of the conductivity is present while the upwinded stencil yields a solution that is monotonic throughout. In the regions where the conductivity varies smoothly, the proposed upwinded stencil yields potential contours that are almost identical to those obtained with the second-order accurate central difference scheme. Because the mesh is rather coarse and the solution is not grid-independent, this is a good indication that the upwinded stencil has an order of accuracy similar to the central-difference stencil at least within regions where the conductivity varies smoothly.

The second-order accuracy of the proposed scheme is confirmed through a grid convergence study. In Fig. 5, both components of the electric field are plotted for 3 different mesh levels: 97×97, and 193×193, and 1537×1537 nodes. The electric field obtained using the finest mesh can be considered to be an essentially exact solution. Indeed, it is ensured that further refining the mesh would not yield a discernible change in the electric field profiles. Then, assuming that the solution on the finest mesh is exact, it is possible to estimate the order of accuracy of the discretization stencil through Richardson extrapolation of the electric field:

$$p \approx \underset{i=1}{\overset{d}{\text{ave}}} \left\{ \ln\left(\frac{\boldsymbol{E}_i^{\text{coarse}} - \boldsymbol{E}_i^{\text{exact}}}{\boldsymbol{E}_i^{\text{fine}} - \boldsymbol{E}_i^{\text{exact}}} \right) \Big/ \ln\left(\frac{\Delta x_i^{\text{coarse}}}{\Delta x_i^{\text{fine}}} \right) \right\} \tag{61}$$

where p is the order of accuracy of the scheme. With the help of the latter equation, and by gathering the solution error on the coarse and fine meshes from Figure 5, the order of accuracy of the method can be estimated. Throughout most of the domain, the order of accuracy of the upwinded scheme can be seen to vary between 1.8 and 1.9. However, close to the discontinuity of the conductivity, the order of accuracy drops to about 1.0. This is not surprising, because the proposed method utilizes a TVD scheme to ensure monotonicity, and TVD schemes are well known to be first-order accurate nearby discontinuities while being second-order accurate in regions where the properties vary smoothly.

8. Conclusions

A variant of the generalized Ohm's law that is applicable to a multicomponent weakly-ionized plasma in a magnetic field is here derived. The proposed formulation takes into consideration the *separate* contributions to the ion slip current originating from the different types of ions. It is shown that the latter can be derived from the charged species momentum and mass conservation equations by making only 3 assumptions. Namely, when compared to the electric field force and the pressure gradient force acting on a charged species, the terms related to momentum diffusion, the terms involving collisions between charged species, and the terms related to the change in inertia are assumed negligible. It is argued that the latter assumptions are valid as long as the gas remains weakly-ionized (that is, the ionization fraction should remain below 10^{-4} or so).

Starting from the multicomponent form of the generalized Ohm's law, an equation for the electric field potential is then determined, that is applicable to a non-neutral plasma with multiple types of ions in the presence of a magnetic field. Despite some similarities between the potential equation and the Poisson equation, it is argued that the discretization of the potential equation cannot be accomplished in the same manner (by using only central differences). Indeed, the discretization of the potential equation is demonstrated to require the use of upwinded stencils in order to yield a solution free of spurious oscillations. The use of upwinded stencils is seen to be necessary when the skew-symmetric terms part of the tensor conductivity matrix predominate over the other terms. This is shown to be the case when three conditions are found *conjunctly*: (i) the Hall parameter is high, (ii) the conductivity exhibits a significant spatial gradient, and (iii) the magnetic field vector has a component perpendicular to both the potential gradient vector and the conductivity gradient vector.

A new discretization stencil for the potential equation is here proposed, spanning 13 grid points in 2D and 33 grid points in 3D. The stencil consists of a minmod TVD upwinded scheme for the skew-symmetric terms and a central difference stencil for the other terms. The stencil is monotonicity-preserving and, in regions where the properties vary smoothly, reaches second-order accuracy. The performance of the proposed upwinded method compared to the standard central-difference scheme is evaluated through several test cases. In all cases, including those with the most stringent conditions, the use of upwinding results in a complete removal of the aphysical oscillations.

Even though upwind differences are only necessary at a high Hall parameter, they are recommended for all flowfields irrespectively of the value of the average Hall parameter. Indeed, even if the Hall parameter remains low on average, it can

attain values well exceeding unity in some flow regions due to Joule heating or some other phenomenon decreasing locally the gas density (on which the Hall parameter inversely depends).

Acknowledgment

This research was supported by the Basic Science Research Program through the National Research Foundation of Korea (NRF) funded by the Ministry of Education, Science and Technology (Grant #2010-0023957).

References

[1] SHNEIDER, M. N., MACHERET, S. O., ZAIDI, S. H., GIRGIS, I. G., AND MILES, R. B., "Virtual Shapes in Supersonic Flow Control with Energy Addition," *Journal of Propulsion and Power*, Vol. 24, No. 5, 2008, pp. 900–915.

[2] KNIGHT, D., "Survey of Aerodynamic Drag Reduction at High Speed by Energy Deposition," *Journal of Propulsion and Power*, Vol. 24, No. 6, 2008, pp. 1153–1167.

[3] ROUPASSOV, D. V., NIKIPELOV, A. A., NUDNOVA, M. M., AND STARIKOVSKII, A. Y., "Flow Separation Control by Plasma Actuator with Nanosecond Pulsed-Periodic Discharge," *AIAA Journal*, Vol. 47, No. 1, 2009, pp. 168.

[4] BENARD, N., BONNET, J. P., TOUCHARD, G., AND MOREAU, E., "Flow Control by Dielectric Barrier Discharge Actuators: Jet Mixing Enhancement," *AIAA Journal*, Vol. 46, No. 9, 2008, pp. 2293.

[5] RIZZETTA, D. P. AND VISBAL, M. R., "Numerical Investigation of Plasma-Based Flow Control for Transitional Highly Loaded Low-Pressure Turbine," *AIAA Journal*, Vol. 45, No. 10, 2007, pp. 2554.

[6] GREENBLATT, D., KASTANTIN, Y., NAYERI, C. N., AND PASCHEREIT, C. O., "Delta-Wing Flow Control Using Dielectric Barrier Discharge Actuators," *AIAA Journal*, Vol. 46, No. 6, 2008, pp. 1554.

[7] SHANG, J. S., "Plasma Injection for Hypersonic Blunt-Body Drag Reduction," *AIAA Journal*, Vol. 40, No. 6, 2002, pp. 1178–1186.

[8] SHNEIDER, M. N., MACHERET, S. O., AND MILES, R. B., "Analysis of Magnetohydrodynamic Control of Scramjet Inlets," *AIAA Journal*, Vol. 42, No. 11, 2004, pp. 2303–2310.

[9] GAITONDE, D. V., "High-Speed Magnetohydrodynamic Flow Control Analyses with Three-Dimensional Simulations," *Journal of Propulsion and Power*, Vol. 24, No. 5, 2008, pp. 946–961.

[10] PARENT, B. AND JEUNG, I.-S., "Fuel-Cell-Powered Magnetoplasma Jet Engine with Electron Beam Ionization," *Journal of Propulsion and Power*, Vol. 21, No. 3, 2005, pp. 433–441.

[11] PARENT, B., MACHERET, S., SHNEIDER, M., AND HARADA, N., "Numerical Study of an Electron-Beam-Confined Faraday Accelerator," *Journal of Propulsion and Power*, Vol. 23, No. 5, 2007, pp. 1023–1032.

[12] FUJINO, T. AND ISHIKAWA, M., "Feasibility of an Onboard Surface Hall Magnetohydrodynamic Power Generator in Reentry Flight," *Journal of Propulsion and Power*, Vol. 25, No. 1, 2009, pp. 83.

[13] WAN, T., CANDLER, G. V., MACHERET, S. O., AND SHNEIDER, M. N., "Three-Dimensional Simulation of the Electric Field and Magnetohydrodynamic Power Generation During Reentry," *AIAA Journal*, Vol. 47, No. 6, 2009, pp. 1327.

[14] SUTTON, G. W. AND SHERMAN, A., *Engineering Magnetohydrodynamics*, Mcgraw-Hill, 1965.

[15] CHAPMAN, S. AND COWLING, T. G., *The Mathematical Theory of Non-Uniform Gases*, Cambridge, 3rd ed., 1970.

[16] D'AMBROSIO, D. AND GIORDANO, D., "Electromagnetic Fluid Dynamics for Aerospace Applications. Part I: Classification and Critical Review of Physical Models," 2004, AIAA Paper 2004-2165.

[17] GIORDANO, D., "Hypersonic Flow Governing Equations with Electromagnetic Fields," 2002, AIAA Paper 2002-2165.

[18] POGGIE, J., "Numerical Simulation of Direct Current Glow Discharges for High-Speed Flow Control," *Journal of Propulsion and Power*, Vol. 24, No. 5, 2008, pp. 916–922.

[19] ROSA, R., *Magnetohydrodynamic Energy Conversion*, Mcgraw-Hill, 1968.

[20] YEE, H. C., KLOPFER, G. H., AND MONTAGNÉ, J.-L., "High-Resolution Shock-Capturing Schemes for Inviscid and Viscous Hypersonic Flows," *Journal of Computational Physics*, Vol. 88, 1990, pp. 31–61.

[21] PEACEMAN, D. W. AND RACHFORD, H. H., "The Numerical Solution of Parabolic and Elliptic Differential Equations," *Journal of the Society for Industrial and Applied Mathematics*, Vol. 3, 1955, pp. 28–41.